Interleaved boost converter efficiency and power density model for active and passive component design

Damien Lemaitre, Jacques Ecrabey

Interleaved Boost Converter Efficiency and Power Density Model for Active and Passive Component Design.

Damien Lemaitre[1], Jacques Ecrabey[1]

[1] Univ. Grenoble Alpes, CEA, Liten, 38000 Grenoble, France

Corresponding author: Damien Lemaitre, damien.lemaitre@cea.fr

Speaker: Damien Lemaitre, damien.lemaitre@cea.fr

Abstract

Interleaved boost converter (IBC) is used in hydrogen vehicle and solar applications. This converter requires a precise model. However, some expressions remain unknown in the state of the art, particularly for discontinuous conduction mode. In this article, the sizing and loss equations for switches, diodes and inductors are described for continuous and discontinuous conduction modes. A simplified method using component libraries for optimal IBC sizing is proposed. The design of a 1.6 kW IBC is carried out. The resulting prototype meets the specifications.

Introduction

Modelling a converter makes its design easier and more efficient. In this article, the converter studied is the interleaved boost (IBC) with uncoupled inductors, as defined in section 1.1.

IBC is widely studied in hydrogen vehicle and solar applications [1]. Key sizing steps are described in the scientific literature. The expression for the input current ripple ΔI_{IN} is described in [1], [2], [3], [4]. Articles [1], [4] also discuss the expression of the output voltage ripple ΔV_{out} in continuous conduction mode (CCM) and discontinuous conduction mode (DCM). The IBC loss model in DCM is described in [3], [5].

The aim of this article is firstly to review the state of the art of known expressions required for IBC sizing. Expressions of root mean square (RMS) currents in DCM components are then defined, which to the author's knowledge are not in the literature. Finally, a simplified sizing method for the IBC is proposed in order to determine the optimum switching frequency f_{sw}, number of legs N_{leg} and components for a given specification.

To achieve these objectives, the operation of the IBC is first described in section 1.

The design equations and the loss model are then discussed in section 2. The IBC sizing method is described in detail in section 3, applied to an example in section 4, and then a prototype is developed and tested in section 5.

The low ripple ΔI_{IN} obtained with the IBC is the main advantage of this topology. For this reason, the example discussed in sections 5 and 6 will focus on the optimal choice of inductors in order to meet the specifications.

1 The Interleaved Boost Converter

This part introduces the notations used to describe the IBC. Its operating principle is then described. The objectives of the IBC model are then discussed.

1.1 Notations

As illustrated in Fig 1 below, the N_{leg} IBC is the combination of N_{leg} boosts electrically connected in parallel, with N_{leg} an integer greater than one. Each leg consists of an inductor and a switching leg, composed of a switch T_k and a diode D_k. We can also use switches instead of diodes for synchronous rectification or when reversibility is required.

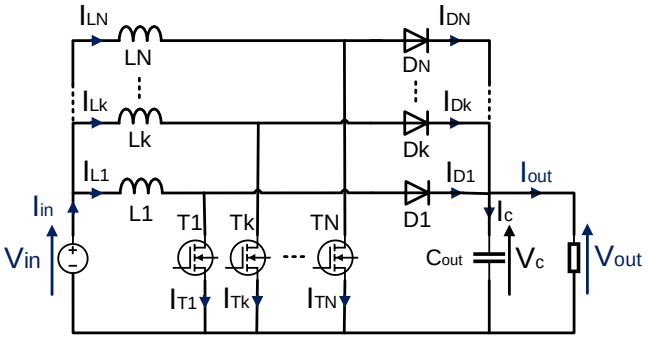

***Fig 1**: Electrical circuit of the interleaved boost converter (IBC).*

The input and output voltages and currents are noted $v_{in}(t), v_{out}(t)$ and $i_{in}(t), i_{out}(t)$. Their mean values are noted V_{in}, V_{out}, I_{in}, I_{out}.

The ripple of the input current $i_{in}(t)$ is noted ΔI_{in}. The ripple of the output voltage $v_{out}(t)$ is noted ΔV_{out}.The voltage and current of the output filter capacitor C_{out} are noted $v_C(t)$ and $i_C(t)$.

The voltages and currents of the inductance L_k, the switch T_k , the diode D_k switches of the k-leg are respectively noted $v_{Lk}(t)$, $v_{Tk}(t)$, $v_{Dk}(t)$ et $i_{Lk}(t)$, $i_{Tk}(t)$, $i_{Dk}(t)$. The current ripple in the inductance L_k is noted ΔI_{Lk}.

1.2 Operation of the Boost Converter

The IBC is a voltage boosting DC/DC converter. To explain how the IBC works, it is therefore necessary to understand how the conventional boost works. Fig 2 below describes the two boost states in CCM.

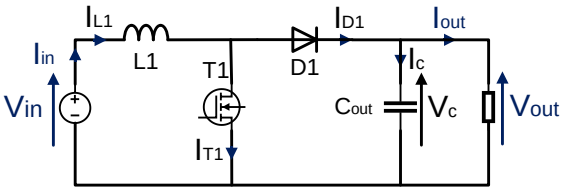

***Fig 2**: Electrical diagram of the boost converter.*

The first state shown in Fig 3 (a) is defined by the ON state of the switch T_1 over the time $[0; \alpha T]$, where α is the duty cycle between 0 and 1. The L_1 inductor stores energy. Diode D_1 is blocked.

The second state shown in Fig 3 (b) occurs when switch T_1 is commanded to turn OFF, i.e. over the time $[\alpha T; T]$ .The diode D_1 conducts and the energy stored in the inductor is transferred to the load.

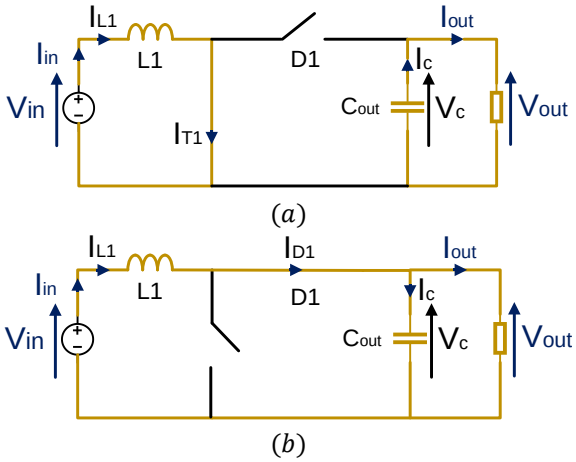

***Fig 3**: Electrical diagram of the boost converter in CCM during phase 1 (a) and during phase 2 (b). Current flow is shown in yellow.*

The waveforms obtained for the currents in the inductor $i_{L1}(t)$, the switch $i_{T1}(t)$ and the diode $i_{D1}(t)$ are shown in Fig 4 below. It shows that the current $i_L(t)$ in the inductor never cancels out, which is characteristic of CCM.

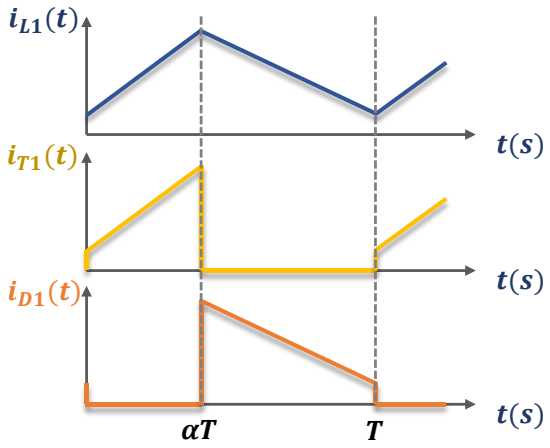

***Fig 4**: Currents in inductor L1, switch T1 and diode D1 of the boost operating in CCM.*

A distinction is made between CCM and DCM according to the value of the inductor current ripple ΔI_L compared to the current in the inductor I_L defined by equation (1).

$$I_L = \langle i_L(t) \rangle = \frac{I_{in}}{N_{leg}} \quad (1)$$

CCM corresponds to the case described by equation (2) and illustrated by Fig 5 (a) below.

$$2\Delta I_L \leq \frac{I_{in}}{N_{leg}} \quad (2)$$

Otherwise, the boost operates in DCM. The current in the inductor then cancels out at a time noted βT and illustrated in Fig 5 (b).

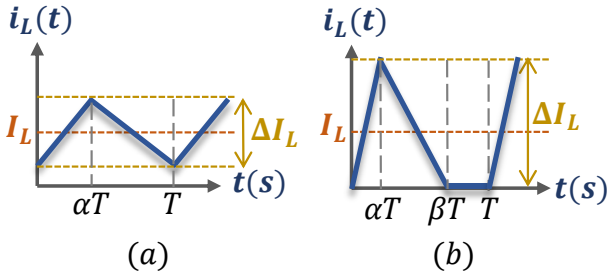

***Fig 5**: IBC inductor current in CCM (a) and DCM (b).*

DCM operation results in a third state during the $[\beta T; T]$ period, with $i_L(t)$ equal to zero. We have explained the boost operation. The next section focuses on the IBC.

1.3 Operation of the IBC

The combination of several boosts in parallel then gives the IBC structure as shown in Fig 1 above. The main advantage of the IBC is that the input current ripple ΔI_{in} can be reduced by increasing the number of legs N_{leg}.

For example, in the case of a three-leg IBC in CCM, a typical shape of the currents $i_{L1}(t)$, $i_{L2}(t)$, and $i_{L3}(t)$ of the leg inductors is shown in Fig 6.

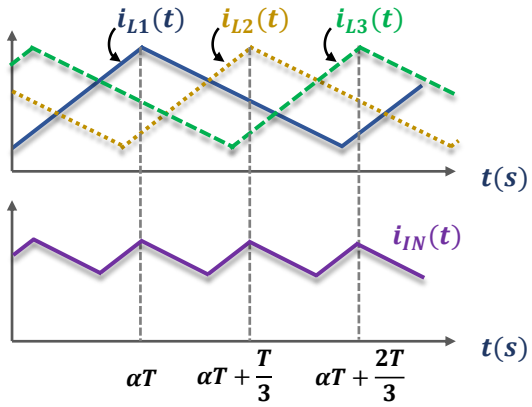

***Fig 6**: Example of the waveforms of the currents in the L1, L2 and L3 inductors of a three-legs IBC.*

The principle is to phase-shift these three currents using switch control in order to reduce ΔI_{in}, as illustrated on Fig 6. The current $i_{in}(t)$ is the sum of the currents in the leg inductances of the IBC.

2 Converter Sizing Model

This section describes the equations used to size IBC components in CCM and DCM. Their voltage and current constraints are defined.

The expressions for the leg inductances and the output capacitor are defined.

2.1 IBC Sizing Model

The quantities with the index X_{Max} represent the maximum stresses of the variable "X". The voltage withstand of switches T_k, diodes D_k inductors L_k and output capacitor are defined by equations (3), (4) and (5). The maximum current withstand is defined by equations (6) and (7). Note that the expression for the current withstand depends on the conduction mode.

$$V_{Tk_{Max}} = V_{Dk_{Max}} = V_{out_{Max}} \quad (3)$$

$$V_{L_{Max}} = \begin{cases} V_{out} - V_{in} & if \ V_{out} > 2V_{in} \\ V_{in} & if \ V_{out} \leq 2V_{in} \end{cases} \quad (4)$$

$$V_{CoutMax} = V_{out} + \frac{\Delta V_{out}}{2} \quad (5)$$

$$I_{Lk_{Max}} = I_{Tk_{Max}} = I_{Dk_{Max}} \quad (6)$$

$$I_{Lk_{Max}} = \begin{cases} \frac{I_{in}}{N_{leg}} + \frac{\Delta I_L}{2} & CCM \\ \Delta I_L & DCM \end{cases} \quad (7)$$

The average currents of switches I_{Tkav}, diodes I_{Dkav} and inductors I_{Lkav} are defined by equations (8), (9), and (10).

$$I_{Lk_{av}} = \frac{I_{in}}{N_{leg}} \quad (8)$$

$$I_{Tk_{av}} = \alpha \frac{I_{in}}{N_{leg}} \quad (9)$$

$$I_{Dk_{av}} = (1 - \alpha) \frac{I_{in}}{N_{leg}} \quad (10)$$

The expression of the RMS current of the components differs between CCM and DCM. In CCM, the RMS currents of switches I_{Tkrms} and diodes I_{Dkrms} are defined by equations (11) and (12). The equation (13) gives the expression of $I_{Tk_{min}}$ and $I_{Dk_{min}}$.

$$I_{Tk_{rms}} = \sqrt{\alpha \left(I_{Tk_{min}} \Delta I_L + \frac{\Delta I_L^2}{3} + {I_{Tk_{min}}}^2 \right)} \quad (11)$$

$$I_{Dk_{rms}} = \sqrt{\frac{V_{in}}{V_{out}} \left(I_{Dk_{min}} \Delta I_L + \frac{\Delta I_L^2}{3} + {I_{Dk_{min}}}^2 \right)} \quad (12)$$

$$I_{Tk_{min}} = I_{Dk_{min}} = \frac{I_{in}}{N_{leg}} - \frac{\Delta I_L}{2} \quad (13)$$

The RMS currents in DCM of switches T_k and diodes D_k are defined by equations (14) and (15).

$$i_{Tk_{rms}} = \sqrt{\frac{2.\Delta I_L.I_{out}.(V_{out}-V_{in})}{3V_{in}N_{leg}}} \quad (14)$$

$$i_{Dk_{rms}} = \sqrt{\frac{2.I_{out}\Delta I_L}{3.N_{leg}}} \quad (15)$$

The RMS current I_{Lkrms} in the L_k inductors is defined in CCM and DCM by the equation (16):

$$I_{Lk_{rms}} = \sqrt{i_{Tk_{rms}}^2 + i_{Dk_{rms}}^2} \quad (16)$$

2.1.1 Inductance Sizing

The value of the leg inductance in CCM is:

$$L_{CCM} = \frac{(V_{out}-V_{in})V_{in}}{f_{sw}V_{out}\Delta I_L} \quad (17)$$

The value of the leg inductance in DCM is:

$$L_{DCM} = \frac{2P_{out}(V_{out}-V_{in})}{N_{leg}f_{sw}V_{out}\Delta I_L^2} \quad (18)$$

The expression of the input current ripple ΔI_{IN} in CCM as a function of the duty cycle and generalized to N_{leg} IBC is given in [3]. This allows us to deduce the ΔI_L expression:

$$\Delta I_L = \frac{\Delta I_{in}N_{leg}\alpha(1-\alpha)}{(N_{leg}\alpha - x)(x+1-N_{leg}\alpha)} \quad (19)$$

$$\frac{x}{N_{leg}} < \alpha < \frac{x+1}{N_{leg}}, x = 0,1,\dots,N_{leg}-1 \quad (20)$$

The expression of ΔI_{IN} in DCM is given for the case $N_{leg} = 3$ in [4]. The expression of ΔI_{IN} generalised to N legs does not appear in scientific literature. Thus, in CCM, the minimum value of the leg inductor is given by equation (21). This is obtained from equations (17) and (19).

$$L_{Min} = \frac{(V_{out}-V_{in})V_{in}}{f_{sw}V_{out}\Delta I_{in}\frac{N_{leg}\alpha(1-\alpha)}{(N_{leg}\alpha - x)(x+1-N_{leg}\alpha)}} \quad (21)$$

Note that the value of L depends on the duty cycle α. Knowing the minimum and maximum duty cycle α_{Min} and α_{Max} of a given application, L_{Min} can be sized more precisely.

The expressions for the output voltage ripple in CCM and DCM are given in [4]. The expression for the output capacitor is derived directly from this.

The electrical constraints of the components, as well as inductor and output capacitor values are now defined. Section 2.2 below discusses the IBC loss model.

2.2 IBC Loss Model

2.2.1 Inductor Losses

The losses P_L in the inductor are composed of the losses in the magnetic core P_{core} and the losses in the winding P_{wind} (22) :

$$P_L = P_{core} + P_{wind} \quad (22)$$

The losses in the magnetic core P_{core} are given by the Steinmetz formula (23).

$$P_{core} = Kf_{sw}^{\alpha}B_{pp}^{\beta} \quad (23)$$

This expression has the advantage of estimating core losses from datasheet data. Note that this formula considers sinusoidal magnetic flux density excitation with no DC component. However, the DC component affects the value of the Steinmetz parameters [6]. This may explain the difference between the estimated and actual losses of the magnetic core. The improved General Steinmetz Equation iGSE can also be used [7].

The losses in the inductance P_{wind} are composed of losses due to the skin effect P_{skin} and losses due to the proximity effect P_{prox}.

$$P_{wind} = P_{skin} + P_{prox} \quad (24)$$

The P_{wind} loss model is described for a round wire and for a Litz wire in [8], [9], [10].

2.2.2 Diode Losses

The diode losses P_{Dk} are composed of conduction losses P_{Dkcond} and reverse recovery losses P_{Dkrr} define in equation (26) and (27) [11].

$$P_{Dk} = P_{Dk_{cond}} + P_{Dk_{rr}} \quad (25)$$

$$P_{Dkcond} = V_{Do} I_{Dav} + R_D I^2_{D_{rms}} \quad (26)$$

$$P_{Dkrr} = \frac{1}{4} Q_{rr} V_{Drr} \quad (27)$$

With the diode on-state resistance R_D, the diode on-state zero-current voltage V_{Do}, the voltage across the diode during reverse recovery V_{Drr}, and the reverse recovery charge Q_{rr}.

2.2.3 MOSFET Losses

Losses P_{Tk} in switches T_k define in equation (28) is composed of conduction losses P_{Tkcond} and switching losses P_{Tksw} define in (29) and (30):

$$P_{Tk} = P_{Tk_{cond}} + P_{Tk_{sw}} \quad (28)$$

$$P_{Tk_{cond}} = R_{DSon} I^2_{Tkrms} \quad (29)$$

$$P_{Tksw} = P_{Tkon} + P_{Tkoff} \quad (30)$$

P_{Tkcond} depends on drain-source on-state resistance R_{DSon} and on the RMS switch current I_{Tkrms}. The switching losses of switches T_k are composed of switch-on and switch-off losses, defined by equations (31) and (32).

$$P_{Tkon} = f_{sw} E_{on}(I_{ds}) K_{on} \quad (31)$$

$$P_{Tkoff} = f_{sw} E_{off}(I_{ds}) K_{off} \quad (32)$$

Where E_{on} and E_{off} are the energies lost when the switch T_k opens and closes. The expressions for the coefficients K_{on} and K_{off} are given below.

$$K_{on} = \frac{V_{ds}}{V_{dsth}} \frac{E_{on}(R_g)}{E_{on}(R_{gth})} \frac{E_{on}(T_j)}{E_{on}(T_{jth})} \quad (33)$$

$$K_{off} = \frac{V_{ds}}{V_{dsth}} \frac{E_{off}(R_g)}{E_{off}(R_{gth})} \frac{E_{off}(T_j)}{E_{off}(T_{jth})} \quad (34)$$

V_{ds} is the drain-to-source voltage, R_g the gate resistor, T_j the junction temperature. The quantities with the index X_{th} represent the theoretical value of the variable "X" considered in the datasheet for calculating switching energies.

All the parameters are shown in the datasheet. The only missing data is the expression of the $E_{on}(I_{ds})$ and $E_{off}(I_{ds})$ functions. The equations can be obtained by fitting the curves from the datasheet, as shown in Fig 7 below.

An approximation by a third-order equation is recommended, the coefficients $A_{on}, B_{on}, C_{on}, D_{on}$, $A_{off}, B_{off}, C_{off}, D_{off}$ are thus introduced:

$$E_{on} = A_{on} I^3_{DS} + B_{on} I^2_{DS} + C_{on} I_{DS} + D_{on} \quad (35)$$

$$E_{off} = A_{off} I^3_{DS} + B_{off} I^2_{DS} + C_{off} I_{DS} + D_{off} \quad (36)$$

To obtain these coefficients, the curve fitting can be carried out, for example, using the online software [12].

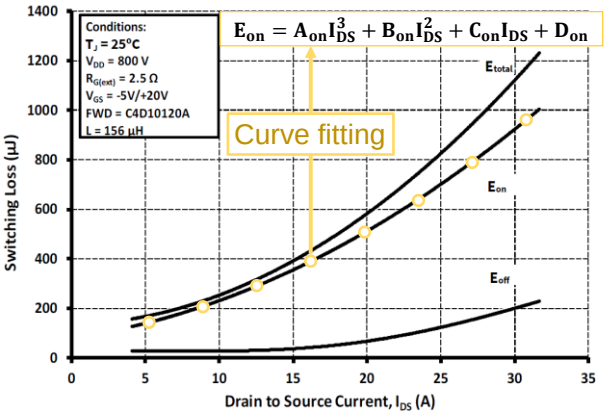

Fig 7: Example of curve fitting of the Eon, function of drain to source current I_{DS} for the C2M0080120D MOSFET.

The losses in the switches, diodes and inductances of the IBC can thus be calculated in CCM and DCM. The choice of the inductance and output capacitor values is dealt with in the next section.

In this section, the principle of the IBC sizing algorithm is first described. Then the set-up stage is detailed. The final selection of components by the algorithm is then discussed.

3 IBC Sizing Method

3.1 Principle

This method has three objectives. The first one is to comply with the ripple constraints on ΔI_{in} and ΔV_{out} defined in the specifications. The second one is to define the best values of N_{leg}, f_{sw}, and ΔI_L to find the optimal solution between the converter's efficiency and volume.

The third objective is to select the components from the libraries set up beforehand. Fig 8 below shows the process method to follow for an optimal IBC sizing.

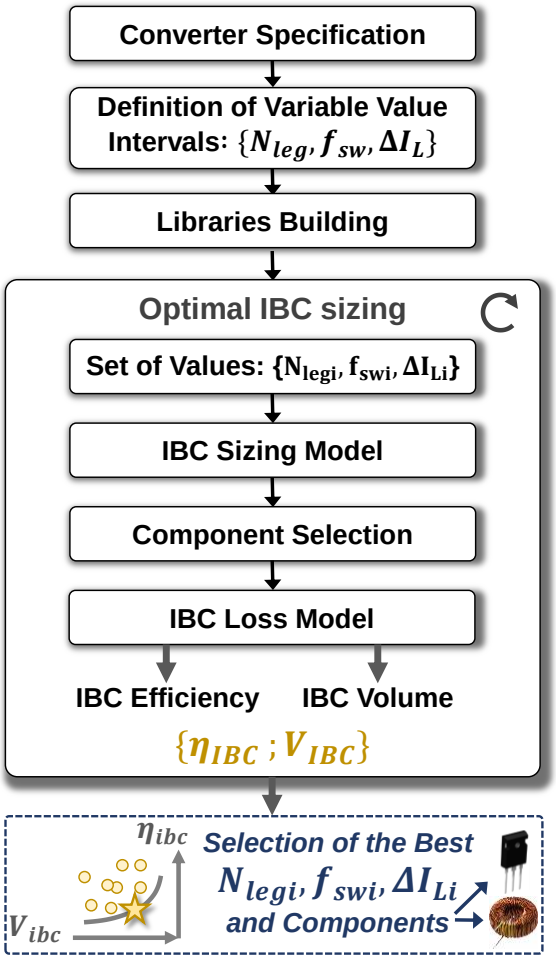

***Fig 8**: Method description for optimal IBC sizing.*

The converter specifications are the rated output power P_{out}, the rated input and output voltages V_{in} and V_{out}, the switching frequency f_{sw}, the minimum and maximum duty cycle α_{Min} and α_{Max}, the maximum ripples of the input current ΔI_{in} and output voltage ΔV_{out}.

Then, several sets of parameters $\{N_{leg}, f_{sw}, \Delta I_L\}$ can provide interesting dimensioning. We therefore need to define the limits of these variables. Yet, as shown in the IBC sizing model section 3.1, component current constraints depend on the number of legs N_{leg} and ΔI_L. It is therefore preferable to have at least one switch, diode and inductor that is neither undersized nor oversized for each value of N_{leg}. This is to ensure that the optimisation is as relevant as possible. If the switching frequency range is large, the same consideration on components with regard to frequency can be applied.

The following section describes how to build component libraries

3.2 Libraries Building Example

The objective of the library of a component is to be able to provide it as input to the IBC loss model in order to obtain the losses, and the volume.

Let us consider the MOSFET library as an example. Each MOSFET must contain the following information: V_{dsMax}, I_{dsMax}, R_{DSon}, $E_{on}(R_g)$, $E_{on}(R_{gth})$, $E_{on}(T_j)$, $E_{on}(T_{jth})$, A_{on}, B_{on}, C_{on}, D_{on}, A_{off}, B_{off}, C_{off}, D_{off}. The volume $V_{cooling}$ of the active component cooling system is often considerable, hence it is advisable to specify it. Likewise, the losses $P_{cooling}$ associated with the energy it consumes.

The same principle must be followed with the diode library and inductor library, incorporating the characteristics involved in its loss model as described in section 2.2.

It is also possible to fix the choice of some components, while allowing multiple alternatives for the others. This scenario is applied in the section 4.

3.3 Component Selection

The selection of components can be carried out in several ways. The chosen method is to retain all components meeting the electrical constraints calculated during the sizing model of the IBC, as illustrated in Fig 8. This approach increases computation time but ensures no solution is omitted as a result. The method described here is applied in the following section. The resulting outcome will be implemented and experimentally tested in section 5.

4 Application Case

The IBC specifications to be designed are described in section 4.1. The influence of the inductor current ripple ΔI_L is then outlined in section 4.2. The selection of the optimal sizing of the IBC is carried out in section 4.3 among all the solutions.

4.1 Specifications

In this example, the study focuses on the inductance sizing.

The objective is to determine if the described IBC model allows meeting the set constraint on the input current ripple ΔI_{in}. The optimal point respecting the specifications will be selected.

The fast prototyping platform Imperix [13] will be used to implement the converter once sized. It consists of commercial switching arms, each composed of two MOSFETs C2M0080120D. Therefore, the choice of switches and diodes is predetermined. Table 1 presents the specifications considered for the IBC sizing.

P_{out}	$1600\ W$
V_{in}	$400\ V$
V_{out}	$500V\ -\ 700\ V$
α_{Min}	0.2
α_{Max}	0.45
ΔI_{in}	$< 10\%\ I_{in}$
f_{sw}	$[10kHz; 30kHz; 50kHz; 70kHz; 90kHz]$
N_{leg}	$[1; 2; 3; 4]$

***Table 1**: Specifications considered for the IBC sizing in the application case studied.*

The volume of the switches, heatsinks, fans and output capacitors of the Imperix legs is known. With the inductor volume known, the converter's power density can be calculated directly. However, if the Imperix modules allow rapid production of the converter, there are oversized for the present specifications. Consequently, it is more relevant to consider the inductors volume only, what is done in this study.

Note that the input voltage V_{in} is fixed at 400V while the output voltage V_{out} can vary between 500V and 700V, implying duty cycle ratios α_{Min} and α_{Max} of 0.2 and 0.45 respectively.

In the current scenario, the inductances are sized for each set of values of the variables N_{leg},f_{sw},ΔI_L using an algorithm. The inductance library is thus replaced by a library of ETD magnetic cores of whose sizes are ETD 29, 34, 39, 44, and 59.

4.2 Influence of the Current Ripple

The maximum imposed on the input current ripple ΔI_{in} limits the allowable current ripple ΔI_L in the inductors. Due to the interleaving of legs, the limit on ΔI_L relaxes as the number of legs increases. This is illustrated in Fig 9 below. The losses Fig 9 (a) and the volume of the IBC Fig 9 (b) are plotted as a function of ΔI_L, for N_{leg} ranging from 1 to 4.

The switching frequency f_{sw} considered in this case is 50 kHz. Solutions meeting the constraint $\Delta I_{in} < 10\%\ I_{in}$ are located in the green regions, marked with the "✓" indicator. Other solutions do not meet this condition and are therefore not acceptable.

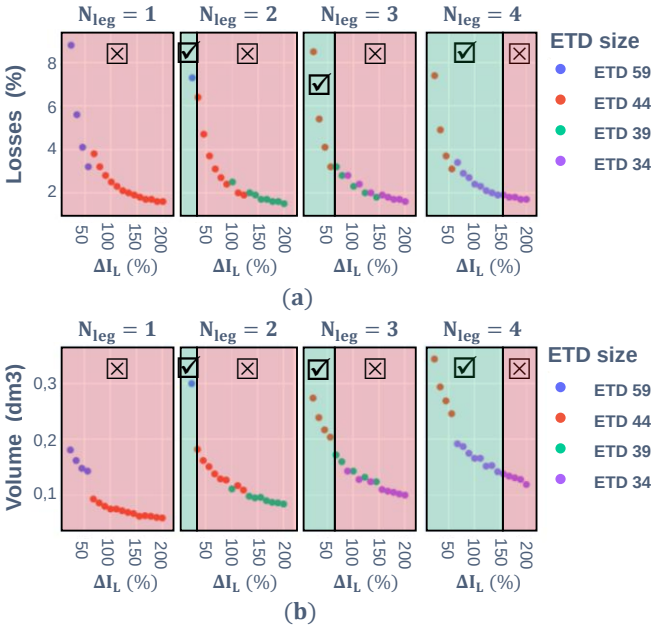

***Fig 9:** IBC Losses (a) and inductor volume (b) of the IBC as a function of the current ripple in the inductors ΔI_L (in percentage of the current inductor I_L), the number of legs N_{leg}, and the magnetic core constituting the inductors. Only solutions within the region marked by the "✓" indicator meet the condition: $\Delta I_{in} < 10\%\ I_{in}$. The switching frequency is 50 kHz.*

Fig 9 shows that no solution exists for $N_{leg} = 1$. In this case, the ripple ΔI_L is equal to ΔI_{in}, imposing a low inductor current ripple ΔI_L: $\Delta I_L < 10\%\ I_{in}$. This requires a high inductance value L, implying a peak induction in the core greater than the tolerated value. Fig 9 shows that increasing ΔI_L leads to a reduction in the losses of the IBC as well as the total inductors volume reduction. This allows a reduction in the inductance value. Consequently, it enables to select smaller magnetic cores and/or cores with fewer turns.

In addition, to increase ΔI_L reduces the value of the magnetic field seen by the core and the turns, consequently reducing losses. Increasing the number of legs allows to increase ΔI_L while still respecting the limit on ΔI_{in}. This explains why the optimal solution, with the selected criteria, is achieved for $N_{leg} = 4$.

The maximum inductor current ripple allowable is 150% in this case, as illustrated in Fig 9.

Fig 10 (a) and Fig 10 (b) below show the IBC losses and inductors volume as a function of the current ripple ΔI_L for $N_{leg} = 4$ and a switching frequency f_{sw} of 50 kHz.

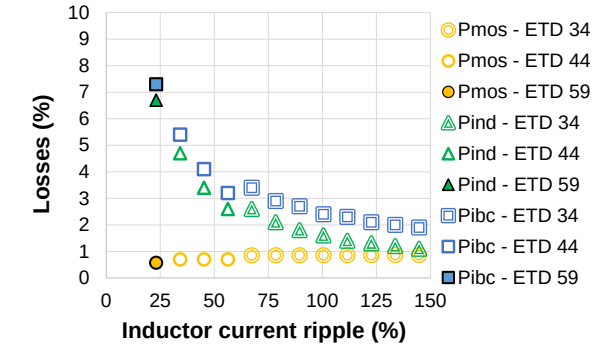

(a)

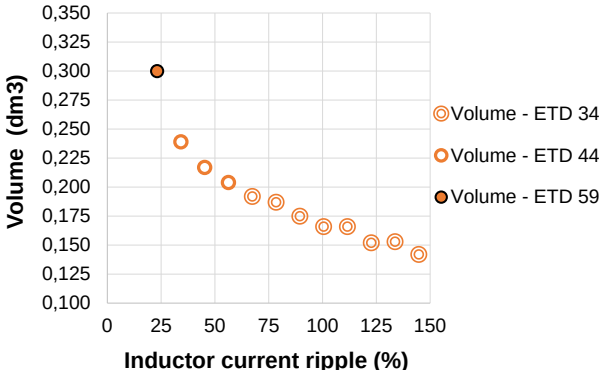

(b)

***Fig 10**: IBC losses (a) and IBC inductor volume (b) as function of the inductor current ripple ΔI_L (in percentage of the current inductor I_L). The switching frequency is 50 kHz and the leg number is 4.*

Fig 10 (a) and Fig 10 (b) clearly demonstrate the influence of ΔI_L on the choice of the magnetic core, thereby impacting the IBC losses and the inductors volume.

The influence of the current ripple ΔI_L and the legs number N_{leg} on the IBC losses and inductors volume. We will now see all the solutions with the switching frequency as an additional variable.

4.3 Selected Solution

Fig 11 below illustrates the various IBC designs that meet the specifications. The variables are the legs number N_{leg}, the switching frequency f_{sw} and the inductor current ripple ΔI_L.

The converter losses are plotted as a function of the inductors volume. The values of variables N_{leg} and f_{sw} are classified in Fig 11 (a). The ETDs used are distinguished in Fig 11 (b).

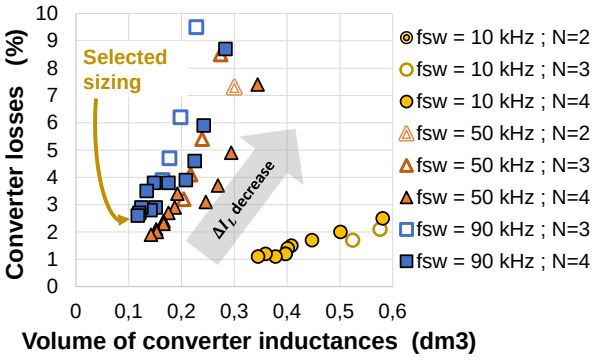

(a)

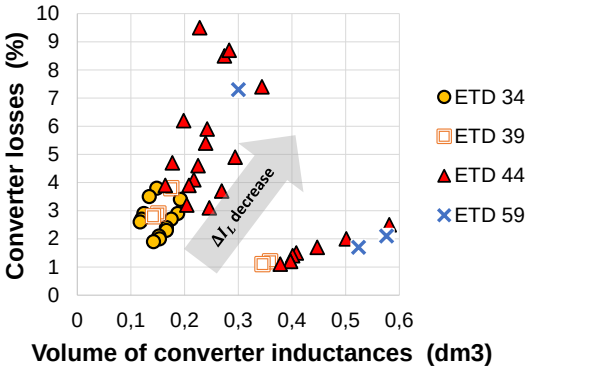

(b)

***Fig 11**: Converter losses as function of inductors volume with solutions classified by switching frequency and number of legs (a), then sorted by the size of ETDs used (b).*

The selected IBC sizing is indicated in Fig 11 (a) and detailed in Table 2 below. The specifications of the required inductors are detailed in Table 3 below.

f_{sw}	N_{leg}	ETD	ΔI_L
90 kHz	4	ETD 34	145 %
P_{mos}	P_{ind}	V_{ind}	η_{ibc}
1,5 %	1,2 %	117 cm^3	97,3 %

***Table 2**: Sizing parameters of the optimal IBC as indicated in Fig 11 (a).*

L	air gap	R_{wire}	N_t
1.33 mH	0.77 mm	0.25 mm	95

***Table 3**: Characteristics of the four inductors of the optimal IBC in Fig 11 (a).*

Now that the IBC optimal sizing is known, the objective of the next section is to compare these theoretical results with those measured on the prototype.

5 Experimental Results

In this part, the IBC with the characteristics detailed in Table 2 and Table 3 above is realised and tested.

5.1 Converter Making

Fig 12 below shows the inductors made with the characteristics of Table 3. With these inductors and the switching legs of the Imperix PEB8024 modules, the four-leg IBC is made and illustrated in Fig 13.

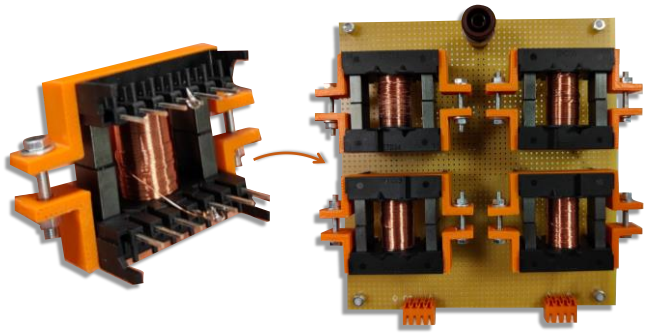

***Fig 12**: Optimised inductance on the left. Inductance of the 4 IBC legs on the right.*

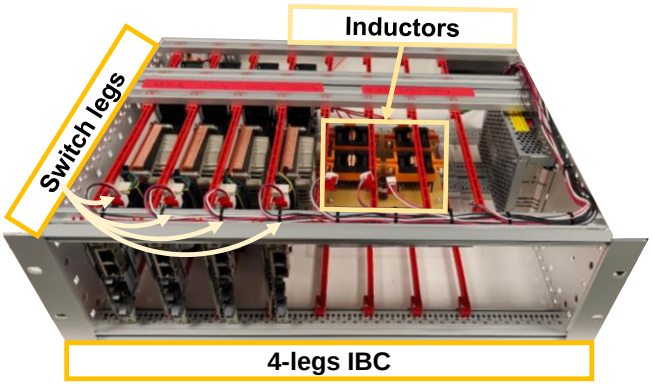

***Fig 13**: IBC made with Imperix switching legs and the sized inductors.*

5.2 Measures

The inductance currents of the four legs of the IBC and the input and output currents are measured using the CP031 current probe. HVD3106 and ADP305 differential probes measure input and output voltages respectively.

The ripple of the input current is measured on a Wavesurfer 3024 oscilloscope using cursors.

To calculate efficiency, input and output voltages are measured using Keysight 34450A multimeters. The input and output currents are measured with Fluke 287 multimeters.

The input and output powers are then calculated, enabling the efficiency to be deduced. The converter test bench is shown in Fig 14.

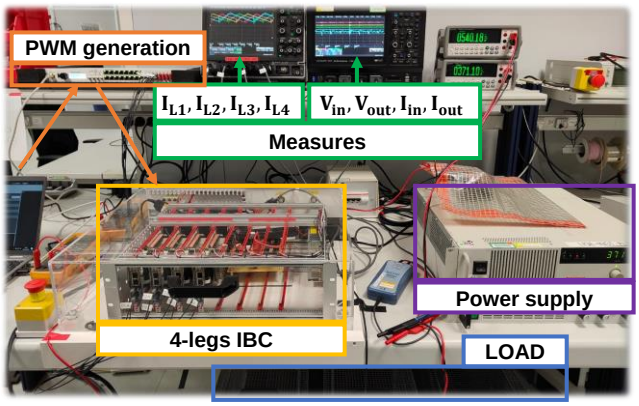

***Fig 14**: IBC test bench*

The specifications considered imply a variable output voltage from 500 V to 700 V. For this reason, tests n°1 and n°3 are carried out close to these operating points. Test n°2 is an intermediate point. Table 4 below shows the characteristics measured for these three cases.

	Test n°1	Test n°2	Test n°3
V_{IN} (V)	400.67	377.94	379.30
I_{IN} (A)	4.02	4.03	4.03
V_{out}(V)	490.50	550.12	670.52
I_{out} (A)	3.21	2.68	2.19
P_{in} (W)	1610.69	1523.10	1527.82
P_{out} (W)	1574.51	1474.32	1468.44
P_{IBC} (W)	36.18	48.78	59.38
η_{IBC} (%)	97.75	96.80	96.11
α	0.27	0.40	0.52
ΔI_{IN} (A)	0.240	0.246	0.202
ΔI_{IN} (%)	5.97	6.11	5.01

***Table 4**: Measurements of characteristics of the 1.6 kW IBC characteristics for three operating points.*

The estimated efficiency at operating point n°3 is 97.3%, compared to 96.11%. This results in a difference of 18W. Output capacitors losses not included in the model can be partly responsible of this difference. In addition, Imperix switching legs operate at a low current considering their characteristics. The losses for a switch current of 1 A are extrapolated from Fig 7, as manufacturer data are not available for currents below 4 A.

The ripple of the input current ΔI_{IN} is lower than 10% of I_{IN} in all three cases. The specifications are thus respected.

Conclusion

The sizing of the interleaved boost converter (IBC) as well as its loss model was addressed in continuous (CCM) and discontinuous (DCM) conduction mode. The proposed IBC sizing method based on component libraries was applied. The 1.6 kW prototype realized complies with the specifications including the constraint on the ripple of the input current ΔI_{in}. In the case studied, only inductors libraries were used. If the switches and output capacitors being imposed, the approach is the same with these components.

The maximum ripple ΔI_{in} measured is 6.11% of the continuous value I_{in}, less than the 10% set in specifications.

Outlook

The addition to the presented model of the volume and losses of the input and output filters, including EMC filters and the component cooling system, is a continuation of this work.

Acknowledgment

Thanks to the “Recherches Technologiques de Base” programme of the French Agency for National Research (ANR) and “CARNOT” program which supported this work with Carnot funding.

References

[1] G. R. Chandra Mouli, J. H. Schijffelen, P. Bauer, et M. Zeman, « Design and Comparison of a 10-kW Interleaved Boost Converter for PV Application Using Si and SiC Devices », *IEEE J. Emerg. Sel. Top. Power Electron.*, vol. 5, nº 2, p. 610-623, juin 2017, doi: 10.1109/JESTPE.2016.2601165.

[2] S. Kascak, M. Prazenica, M. Jarabicova, et R. Konarik, « Four Phase Interleaved Boost Converter: Theory and Applications », vol. 13, 2018.

[3] H. Wang, « Design and control of a 6-phase Interleaved Boost Converter based on SiC semiconductors with EIS functionality for Fuel Cell Electric Vehicle », phdthesis, Université Bourgogne Franche-Comté, 2019. Consulté le: 20 juin 2023. [En ligne]. Disponible sur: https://theses.hal.science/tel-02185678

[4] G.-Y. Choe, J.-S. Kim, H.-S. Kang, et B.-K. Lee, « An Optimal Design Methodology of an Interleaved Boost Converter for Fuel Cell Applications », *J. Electr. Eng. Technol.*, vol. 5, nº 2, p. 319-328, juin 2010, doi: 10.5370/JEET.2010.5.2.319.

[5] D.-D. Tran, S. Chakraborty, Y. Lan, M. E. Baghdadi, et O. Hegazy, « NSGA-II-Based Codesign Optimization for Power Conversion and Controller Stages of Interleaved Boost Converters in Electric Vehicle Drivetrains », *Energies*, vol. 13, nº 19, Art. nº 19, janv. 2020, doi: 10.3390/en13195167.

[6] J. Muhlethaler, J. Biela, J. W. Kolar, et A. Ecklebe, « Core Losses Under the DC Bias Condition Based on Steinmetz Parameters », *IEEE Trans. Power Electron.*, vol. 27, nº 2, p. 953-963, févr. 2012, doi: 10.1109/TPEL.2011.2160971.

[7] K. Venkatachalam, C. R. Sullivan, T. Abdallah, et H. Tacca, « Accurate prediction of ferrite core loss with nonsinusoidal waveforms using only Steinmetz parameters », in *2002 IEEE Workshop on Computers in Power Electronics, 2002. Proceedings.*, Mayaguez, Puerto Rico: IEEE, 2002, p. 36-41. doi: 10.1109/CIPE.2002.1196712.

[8] K. Umetani, S. Kawahara, J. Acero, H. Sarnago, O. Lucia, et E. Hiraki, « Analytical Formulation of Copper Loss of Litz Wire With Multiple Levels of Twisting Using Measurable Parameters », *IEEE Trans. Ind. Appl.*, vol. 57, nº 3, p. 2407-2420, mai 2021, doi: 10.1109/TIA.2021.3063993.

[9] R. P. Wojda et M. K. Kazimierczuk, « Winding Resistance and Power Loss of Inductors With Litz and Solid-Round Wires », *IEEE Trans. Ind. Appl.*, vol. 54, nº 4, p. 3548-3557, juill. 2018, doi: 10.1109/TIA.2018.2821647.

[10] C. R. Sullivan et R. Y. Zhang, « Analytical model for effects of twisting on litz-wire losses », in *2014 IEEE 15th Workshop on Control and Modeling for Power Electronics (COMPEL)*, Santander: IEEE, juin 2014, p. 1-10. doi: 10.1109/COMPEL.2014.6877187.

[11] Infineon, « MOSFET Power Losses Calculation Using the DataSheet Parameters ».

[12] « Curve fitting software ». [En ligne]. Disponible sur: https://plotdigitizer.com/app

[13] « Power electronic solutions for teaching, research and the industry - imperix ». [En ligne]. Disponible sur: https://imperix.com/solutions/